Research Article Vol. 7, No. 8 / August 2020 / Optica 1007

optica

Multifocus off-axis zone plates for x-ray free-electron laser experiments

Florian Döring,* Benedikt Rösner, Manuel Langer, Adam Kubec, Armin Kleibert, Jörg Raabe, Carlos A. F. Vaz, Maxime Lebugle, and Christian David

Paul Scherrer Institut, Villigen-PSI 5232, Switzerland
**Corresponding author: florian.doering@psi.ch*

Received 26 May 2020; revised 2 July 2020; accepted 7 July 2020 (Doc. ID 398022); published 14 August 2020

X-ray free-electron lasers (XFELs) are paving the way towards new experiments in many scientific fields, such as ultrafast science, nonlinear spectroscopy, and coherent imaging. However, the strong intensity fluctuations inherent to the lasing process in these sources often lead to problems in signal normalization. In order to address this challenge, we designed, fabricated, and characterized diffractive x-ray optics that combine the focusing properties of a Fresnel zone plate with the beam-splitting capability of a grating in a single diffractive optical element. The possibility to split the incident beam into identical copies allows for direct shot-to-shot normalization of the sample signal, thereby greatly enhancing the signal-to-noise ratio in experiments with XFEL radiation. Here we propose two schemes for the design of such diffractive x-ray optical elements for splitting and focusing an incoming beam into up to three foci by merging a grating with a focusing zone plate. By varying the duty cycle of the grating or the relative shift of the Fresnel zone plate structure, we are able to tune the relative intensities of the different diffraction orders to achieve the desired splitting ratios. Experimental confirmation of the design is provided with soft x-ray light (540 eV) and shows a good agreement with calculations, confirming the suitability of this approach for XFEL experiments.

https://doi.org/10.1364/OPTICA.398022

1. INTRODUCTION

X-ray free-electron lasers (XFELs) are currently among the most advanced light sources in the world. The possibility to generate extremely short pulses of high brilliance with high degree of coherence from the extreme ultraviolet (EUV) regime up to hard x-rays is outstanding and unique [1–3]. In this energy range, many electronic transitions in matter can be probed, providing access to ultrafast phenomena on the nanoscale [4]. Moreover, due to the high intensity and short pulse lengths of XFEL shots, new research opportunities open up in multiphoton interactions and ultrafast processes on the femtosecond timescale. For example, interactions of the electronic system with more than just one photon during the lifetime of an excited core-hole state can be studied in the femtosecond regime [5]. It has thus become possible to apply multi-excitation spectroscopy techniques that combine the selectivity and sensitivity of x-rays with the high intensity and short pulse lengths of XFEL light, suitable for studying dynamic processes in the nonlinear regime [6–8].

Although spectroscopy at XFELs promises exciting new insights in many fields of science, its application is challenging and not straightforward [9,10]. Due to the characteristic shot-to-shot intensity fluctuations of XFELs, accurate detection schemes with a high correlation are needed upstream and downstream of the sample for every individual pulse. Moreover, the fact that the intensities of XFEL pulses are typically very high rules out some detection methods (e.g., photoelectron measurements because of nonlinear space charge effects) and requires a high dynamic range. As a result, normalization of the incoming radiation is mostly performed in an indirect way, either by using spectrometers placed upstream and downstream of the sample, or by splitting the beam with a mirror placed halfway in the beam [8,11]. These methods usually suffer from the fact that the correlation of the reference and the signal after the sample can be affected by pointing instabilities, distortions during beam transport, optical aberrations, diffraction fringes, or other changes in the incoming beam on its optical path.

An elegant normalization scheme yielding excellent correlation between the beam intensities can be obtained by the use of a transmission grating as a beam splitter. Compared to a splitting mirror, it has the advantage that pointing instabilities in the beam do not affect the splitting ratio, as only the relative intensity changes as a function of diffraction efficiency, and the incoming spatial intensity distribution is conserved in all diffraction orders. The ratio of intensities in the various diffraction orders is an intrinsic property of the grating structures and largely insensitive to alignment of the transmission grating. Such gratings have been successfully implemented for absorption spectroscopy experiments at LCLS, SACLA, and FLASH [12–14] by placing the sample in one of the diffraction orders and using another as a reference. The drawback

of this approach is that an additional diffraction grating in an optical setup decreases its overall efficiency, increases absorption losses, and makes alignment more challenging.

Here we overcome these problems by designing an optical element that combines the functionalities of a focusing off-axis zone plate and a beam-splitting grating in one. Such devices offer a normalization scheme that enables dynamic and spectroscopic experiments with high fluences and precise signal normalization on a shot-to-shot basis. Related approaches have been pursued to modify the imaging properties of Fresnel zone plate lenses in x-ray microscopy applications to create differential interference contrast [15–19]. We expand on the Chang *et al.* [15,16]. Specifically, we present two schemes for the design of diffractive optical elements providing up to three focal spots, and we present their theoretical description, which allows us to tune the relative intensity of the focal spots. This is of particular relevance for pump probe experiments, as one beam can be used to probe the pumped sample, the second beam probes the unpumped sample, and a third beam provides a reference signal for normalization. To demonstrate the feasibility of three-spot focusing for applications at XFELs, we present the fabrication of these optics from radiation hard material based on our approach. Efficiency measurements show an excellent quantitative agreement with our calculations.

2. OPTICAL DESIGN AND DIFFRACTION THEORY

Combining two functionalities—focusing and beam splitting—in a single optical element can be achieved by superimposing a grating and an off-axis zone plate. The grating splits the beam along one spatial direction, while the positive orders of the zone plate focus the beam in the other spatial direction as illustrated in Fig. 1(a). By using an off-axis zone plate, the zeroth, nonfocusing diffraction order of the focusing functionality is spatially separated from its first, focusing diffraction order, making a central stop and an order-sorting aperture unnecessary for this application. The structures of the off-axis zone plate are oriented, in a first approximation, orthogonal to the lines of the beam-splitting grating. The optical element thus generates a two-dimensional diffraction pattern, and we can assign a pair of diffraction indices (m, n), where m and n denote the diffraction order of the focusing zone plate and the splitting grating, respectively. In this study, we mainly concentrate on the zone plate's first diffraction order ($m = 1$) and compare the intensity distribution of the different diffraction orders of the beam splitter, in line with the application to use multiple focus spot for XFEL experiments. All diffraction efficiencies referred to in this study are thus the relative diffraction efficiencies of the beam splitter in the first, focused diffraction order of the off-axis zone plate. Moreover, we assume the diffracting structure to be binary, meaning that it consists of regions that either open or filled to a certain height with a material having phase-shifting and absorbing properties as described by its complex refractive index $n = 1 - (\delta + i\beta)$. We describe two alternative designs for an off-axis zone plate that contains a superimposed beam-splitter grating. One way to superimpose the grating is the inversion of the open and filled zones of the off-axis zone plate with a predefined periodicity [***pattern inversion***, see Fig. 1(c)], also named the XOR method [Fig. 1(a)]. This has the same effect as stacking an ideal phase grating, meaning a grating inducing a phase shift of π and zero absorption, onto the zone plate. Combining both functionalities in one pattern strongly reduces the losses compared to the actual stacking of a physical grating and a zone plate, which is a great advantage of superimposing the beam-splitting properties by design. The diffraction angle induced by the grating and thus the beam separation in the focal plane is determined by the periodicity of the inversion, corresponding to the grating pitch p and the photon energy.

The duty cycle, meaning the width of the inverted part divided by the inversion period, can be freely adjusted as shown in Fig. 1(d). This affects the efficiency of the beam-splitting functionality as described below. Another way of superimposing the grating and an off-axis zone plate is the shift of the filled zones by a fraction of their period [***pattern shift***, see Fig. 1(e)]. Here the degree of the shift defines the relative intensities of the resulting grating diffraction orders.

In both designs, it is possible to tune the relative intensities in the focal spots, i.e., the efficiency of the grating diffraction orders, by variation of either the duty cycle of the inversion or the zone shift. Especially the efficiency of the grating's undiffracted beam ($n = 0$) can be controlled precisely. In principle, this opens up two special cases: (i) a two-beam scheme, where the undiffracted beam of the grating is suppressed and the first grating orders ($n = \pm 1$) are used for measurement and normalization, respectively, and (ii) a three-beam scheme, where three identical copies of the beam are made available, which is relevant, e.g., for pump-probe experiments.

In order to quantify the effect of both approaches on the relative intensity distribution, we start from the equations for the

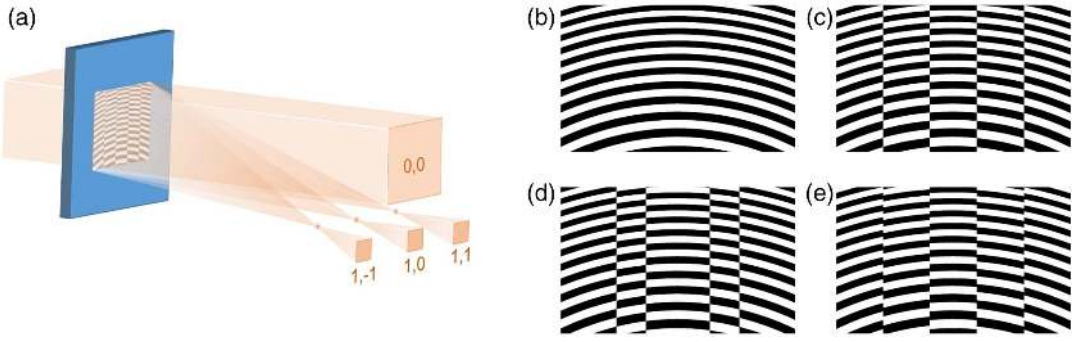

Fig. 1. (a) Geometry of an optical element that combines focusing and splitting, creating multiple focus spots for use in an XFEL experiment. The first index denotes the diffraction order of the focusing zone plate, the second index the order of the splitting grating. (b) Off-axis zone plate without a superimposed grating. (c) Off-axis zone plate combined with a phase grating by periodic inversion of the zone structure (pattern inversion) with a duty cycle $d = 0.5$. (d) Pattern inversion with a grating duty cycle of $d = 0.32$. (e) Zone structures shifted by one quarter of the zone plate period (pattern shift).

diffraction efficiencies of a one-dimensional diffraction grating [20,21]:

$$\frac{I_m(d,k)}{I} = \eta_m = \left[\frac{\sin(dm\pi)}{m\pi}\right]^2 \cdot [1 + \exp(-2kt\beta) - 2\exp(-kt\beta)\cos(kt\delta)](m > 0), \quad (1)$$

$$\frac{I_0(d,k)}{I} = \eta_0 = d^2 + (1-d)^2\exp(-2kt\beta) + 2d(1-d) \times \exp(-kt\beta)\cos(kt\delta)(m = 0), \quad (2)$$

where $I_m(k)$ is the intensity for a diffraction order m, I is the incident intensity, d is the duty cycle (structure width divided by the period), k is the wavenumber, t is the grating line thickness (in beam propagation direction), and β and $1-\delta$ are the imaginary and real parts of the refractive index, respectively. From Eq. (1), it becomes clear that even diffraction orders vanish for a duty cycle of $d = 0.5$, independent of the complex index of refraction of the material or the photon wavenumber. For the zeroth-order signal, a particular duty cycle exists for every grating with π phase shift ($kt\delta = \pi$), where the intensity drops to zero. In the ideal case of a phase grating without absorption, i.e., $\beta = 0$, a duty cycle of $d = 0.5$ leads to a complete suppression of the zeroth and all even orders. For nonzero absorption ($\beta \neq 0$), the duty cycle for zeroth-order suppression deviates from 0.5, while higher even orders still vanish for $d = 0.5$.

We consider two particular cases that will form the basis of our approach, and we focus on the intensity ratio of the $\pm$1st and the zeroth grating diffraction orders that are of most interest here. To illustrate the effect of the duty cycle on the diffracted intensity, we consider the case of an ideal phase grating, where $kt\delta = \pi$ and $\beta = 0$:

$$\frac{I_1(d)}{I} = \eta_1 = 4\left[\frac{\sin(d\pi)}{\pi}\right]^2, \quad (3)$$

$$\frac{I_0(d)}{I} = \eta_0 = (2d-1)^2. \quad (4)$$

These equations describe the situation for the *pattern inversion* approach, where the splitting efficiencies induced by the phase grating depend on the duty cycle of the inversion as shown in Figs. 1(c) and 1(d). This effect is plotted for the zeroth and first diffraction order ($n = 0$ and $n = 1$) in Fig. 2(a).

If the duty cycle is fixed to $d = 0.5$, the phase shift is expressed as $\varphi = kt\delta$, and the trigonometric relation $\sin^2(x) = 1/2(1-\cos(2x))$ is used, we can derive the following expressions for the efficiencies:

$$\frac{I_1(\varphi)}{I} = \eta_1 = 2\left[\frac{\sin(\pi/2)}{\pi}\right]^2 \cdot [1-\cos(\varphi)] = 4\left[\frac{\sin(\varphi/2)}{\pi}\right]^2, \quad (5)$$

$$\frac{I_0(\varphi)}{I} = \eta_0 = (1+\cos(\varphi))/2 = 1-\sin^2\left(\frac{\varphi}{2}\right) = \cos^2\left(\frac{\varphi}{2}\right). \quad (6)$$

These equations describe the situation for the *pattern shift* approach, where the phase shift induced by the grating corresponds to the displacement of the filled zone as a fraction of the periodicity in units of 2π. An inversion represents a translation by half of the periodicity and thus corresponds to a phase shift of $\varphi = \pi$. The resulting diffraction efficiencies for $n = 1$ and $n = 0$ are plotted in Fig. 2(b).

From Fig. 2, it becomes obvious that the function for the zeroth order is different in both cases. It follows a parabola shape as the duty cycle is changed (pattern inversion), while it follows a cosine shape as the filled zones are translated (pattern shift). The first-order functions are the same as can be seen from Eqs. (3) and (5).

In both cases, a duty cycle of $d = 0.5$ or a shift of $\varphi = \pi$ leads to a maximum intensity of $4/\pi^2 \approx 40.5\%$ in each first order and suppresses the zeroth order, which are the parameters where the patterns become identical. This is the desired geometry for splitting the beam in two equally intense copies. For three equally intense copies, the first orders and the zeroth order must have the same intensity, which occurs at the crossing points of the curves. In the inversion case, this point is found at duty cycles $d = 0.27$ and $d = 0.73$, leading to a relative beam intensity in each of the three beams of 21%. In the case of shifted zones, this point occurs at a phase shift of $\varphi = 2 \cdot \text{asin}\left(\pm(\frac{4}{\pi^2}+1)^{-1/2}\right) = 0.32 \cdot 2\pi$ and $0.68 \cdot 2\pi$ at a relative beam intensity of 29%.

So far, we have only considered the case of a one-dimensional phase grating. However, we are interested in the case where the phase grating superimposes an off-axis zone plate. Thus, it is important to investigate whether this leads to significant changes when using two-dimensional optics as a normalization scheme.

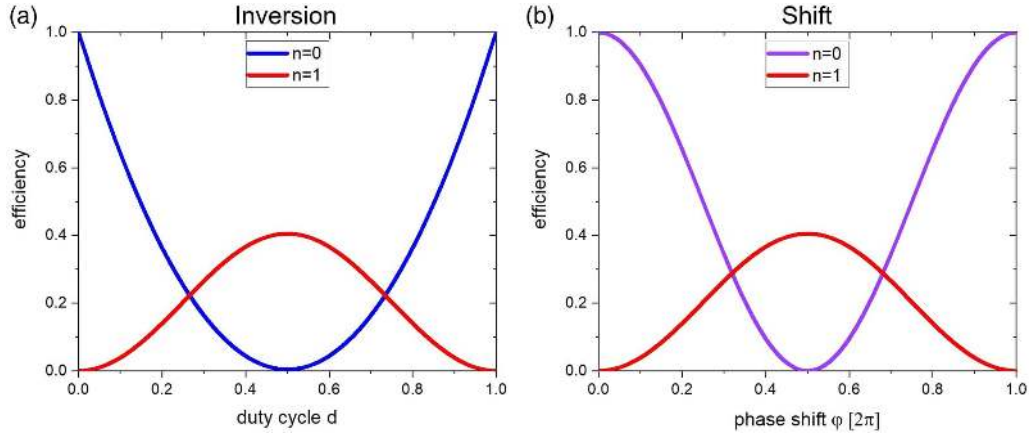

Fig. 2. Calculated efficiencies for a phase grating as a function of (a) duty cycle and of (b) the phase shift with a fixed duty cycle of $d = 0.5$. Note the different course of the zeroth-order functions while the first-order function are the same.

For this purpose, we approximate the zone plate as a grating and treat the whole optic as a two-dimensional grating, which is a good approximation for off-axis zone plates, where the fraction of the zone plate pattern is far from the optical axis. This means that we now have two diffraction duty cycles d_1, d_2, corresponding to the diffraction indices m and n. By integration of the unit cell in the Fourier space, the equation for the intensity $I_{m,n}(k, d_1, d_2)$ for $m \neq 0$, $n \neq 0$ can be derived analogously to the one-dimensional case (see Supplement 1 for a step-by-step-calculation) [19–21]:

$$\frac{I_{m,n}(k, d_1 d_2)}{I} = \eta_{m,n} = \left[\frac{2\sin(d_1 m\pi)\sin(d_2 n\pi)}{m\pi n\pi}\right]^2 \cdot \left[1 + \exp(-2kt\beta) - 2\exp(-kt\beta)\cos(kt\delta)\right]. \tag{7}$$

For our application of a focusing and beam-splitting normalization scheme, we consider the first diffraction order of the zone plate only. Moreover, we want the highest intensity for this first diffraction order, which is achieved for a zone plate duty cycle of $d_1 = 0.5$. Setting $m = 1$ and $d_1 = 0.5$, Eq. (7) becomes identical to Eq. (1). Introducing the pattern shift for this case, the integration of the unit cell in the Fourier space yields (see Supplement 1 for details)

$$\frac{I_{m,n}(k, s, d_2)}{I} = \eta_{m,n} = \left[\frac{2\sin(d_2 n\pi)\sin(s \cdot \pi)}{n\pi^2}\right]^2 \cdot [1 + \exp(-2kt\beta) - 2\exp(-kt\beta)\cos(kt\delta)]. \tag{8}$$

In the case of the three-spot application, we are not only interested in the case of $m = 1$, $n = \pm 1$, but also in the case of $m = 1$, $n = 0$. Here the intensities $I_{1,0}(d_2)$ and $I_{1,0}(s)$ in the *pattern inversion* and *pattern shift* designs can be derived in the same way:

$$\frac{I_{1,0}(k, d_2)}{I} = \eta_{1,0} = \left[\frac{2d_2 - 1}{\pi}\right]^2 \cdot \left[1 + \exp(-2kt\beta) - 2\exp(-kt\beta)\cos(kt\delta)\right], \tag{9}$$

$$\frac{I_{1,0}(k, s)}{I} = \eta_{1,0} = \left[\frac{\cos(s \cdot \pi)}{\pi}\right]^2 \cdot \left[1 + \exp(-2kt\beta) - 2\exp(-kt\beta)\cos(kt\delta)\right]. \tag{10}$$

These equations have the same form as shown in Fig. 2 for the one-dimensional case. Thus, the considerations made above for the one-dimensional phase grating are also applicable for the two-dimensional case, if we compare the relative intensities of the split beam spots in the first diffraction order of the off-axis zone plate.

3. FABRICATION AND OPTICAL PERFORMANCE OF MULTIFOCUS ZONE PLATES

Based on the concept discussed above, we have fabricated a series of multifocus zone plates with various grating duty cycles for the *pattern inversion* and various degrees of movement for the *pattern shift*, keeping the duty cycle of the zone plate at $d = 0.5$ for maximum intensity in the first zone plate order. As discussed above, the grating duty cycle or pattern shift determines the relative intensity between the zeroth and the first diffraction orders of the split beam. Additionally, the grating pitch defines the diffraction angle and thus the angular splitting of the focal spots.

Since we are interested in XFEL applications, we need to use radiation-hard materials such as diamond [22] or silicon [23,24]. The latter can be readily patterned by established processes, moreover, silicon exhibits a large phase shift to absorption ratio δ/β in the EUV region from 30 to 90 eV and in the soft x-ray region between 500 and 1000 eV, which is essential to obtain high diffraction efficiencies. The size parameters for nanostructuring such an optical element are similar to those of an off-axis zone plate as used for time streaking or as analyzer for spectroscopy [8,25–27]. The zone plate diameter, photon energy, and outermost zone width define the focal length, whereas the aperture of the zone plate determines the numerical aperture and thus the diffraction-limited resolution.

In view of future application of the beam-splitting optics for studies on complex materials at the oxygen K-edge, we designed the optical elements for a photon energy of 540 eV [28–30]. The flow of the fabrication process is depicted in Fig. 3. A 1 μm thick single crystalline silicon membrane is coated with a 10 nm chromium layer by thermal evaporation and spin coated with a 70 nm thick polymethylmethacrylate (PMMA) resist layer. The pattern of the diffractive optical element is written into the resist by electron-beam lithography at 100 keV electron energy. The exposed PMMA is removed in a development step, and this pattern is subsequently transferred into the chromium mask by etching the exposed area with a chlorine-based plasma. After removal of the resist in acetone, the pattern is etched ∼650 nm deep into the membrane. The first-order diffraction efficiency of a silicon grating with such structures can be calculated to be 23%; this value is reduced by a factor of 2 due to absorption in the remaining ∼350 nm silicon support. The fact that the optical elements are made from single crystalline silicon makes them tolerant to high radiation loads, as there are no interfaces where layers of different materials could crack or delaminate at elevated temperatures. These monolithic silicon structures are achieved after selective removal of the Cr mask in a final etching step. However, for the here presented experiments at a synchrotron source, we left the Cr mask intact.

Both optical designs (*pattern inversion* and *pattern shift*) were fabricated with different duty cycles and shifts using the process described above. For a better comparison of the inverted and the shifted design, we define the shift s as the displacement of a filled zone related to the local zone plate period (i.e., the width of a transparent and a filled zone pair). For the inversion design, the duty cycles $d = 0$, 0.2, 0.27, 0.32, and 0.5 were fabricated. For the shifted design, the shifts $s = 0$, 0.1, 0.2, 0.27, 0.32, and 0.5 were fabricated. Obviously, the inverted pattern with $d = 0$ is identical to the shifted pattern with $s = 0$ (an off-axis zone plate without modification), and the inverted pattern with $d = 0.5$ is identical to the shifted pattern with $s = 0.5$ [see Fig. 1(c)]. Each off-axis zone plate had a size of 1 mm × 1 mm. The grating pitch (i.e., the periodicity of the pattern modification) was 604 nm, and the outermost zone width of the off-axis zone plate was 230 nm, giving a separation of 0.95 mm between neighboring focal spots and a focal length of 250 mm.

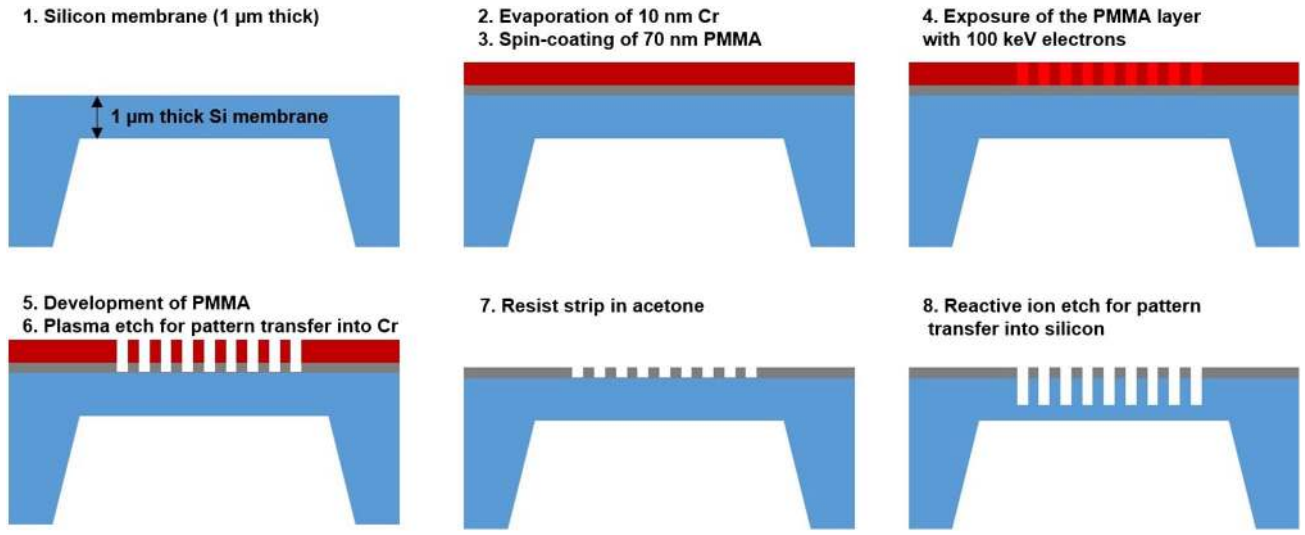

Fig. 3. Fabrication steps for the beam-splitting diffractive optics. The individual steps are described in the figure as well as in the text.

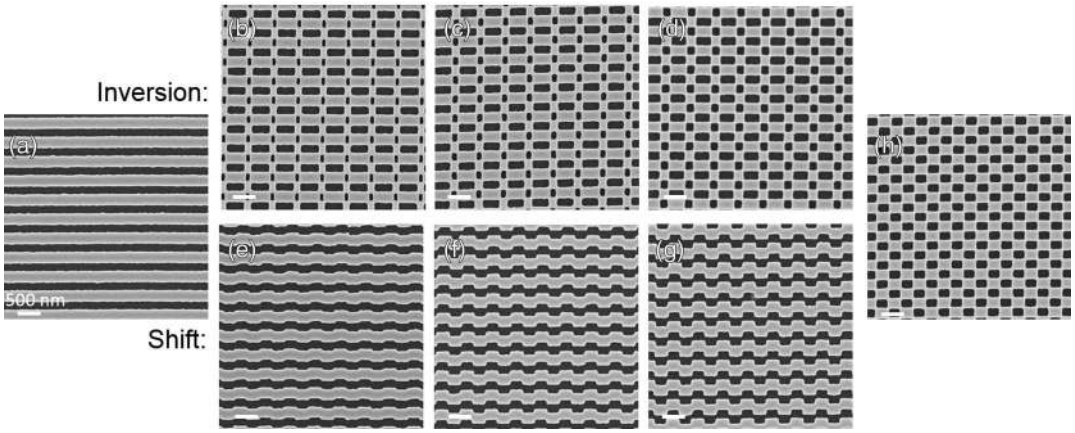

Fig. 4. SEM micrographs of different multispot zone plate designs. The horizontal zone plate structures are superimposed by a phase grating. The grating can be added by inversion of the structures with (a),(b),(c),(d),(h) a defined grating pitch and duty cycle, or (a),(e),(f),(g),(h) by shifting the zones by a defined fraction of the period: (a) $d = 0$, inversion or shift is zero; (b) $d = 0.2$, structure inversion; (c) $d = 0.27$, structure inversion; (d) $d = 0.32$, structure inversion; (e) $s = 0.2$, zone shifting; (f) $s = 0.27$, zone shifting; (g) $s = 0.32$, zone shifting; (h) d = 0.5 or $s = 0.5$; inversion and shift are the same and yield an identical pattern. All scale bars are 500 nm.

Scanning electron micrographs (SEM) of the two types of multifocus zone plate are shown in Fig. 4. Note that in the case of the inversion design an additional fabrication challenge arises. Small duty cycles d result in very narrow structures, which are inherently difficult to fabricate. This challenge evidently becomes more severe with small splitting periods. On the other hand, the shifting strategy suffers considerably less of this effect, because the duty cycle remains at 0.5 in all cases, also for small shifts s, and no features smaller than the half-pitch of the diffracting structures need to be produced.

The multifocus zone plates were characterized at the SIM beamline at the Swiss Light Source (SLS) [31,32] at 540 eV photon energy. The diffraction pattern, as outlined in Fig. 1(a), was imaged with a MÖNCH detector [33]. In Fig. 5, we show the intensity profile generated by the different multifocus zone plates. The images show the nondiffracted, transmitted beam ($m = n = 0$) as large square and the different focused beam copies ($m = 1$, $n = -2 \ldots +2$) as small squares as sketched in Fig. 1(a). The experimental results also confirm that the duty cycle and shift of the grating determines the relative intensities of the different focal spots. As predicted by the calculations, three equally intense spots can be achieved using the inversion design and a duty cycle of $d = 0.27$ [Fig. 5(c)] or $s = 0.32$ [Fig. 5(h)] and two equally intense spots by suppressing the zeroth grating order for $d = s = 0.5$ [Fig. 5(e)]. The integrated spot intensities plotted in Figs. 5(j) and 5(k) reveal the excellent agreement between the measured data with the theoretical curves. Please note that the higher grating orders are more effectively suppressed with the *pattern shift* method. In a three-spot application, the pattern shift approach hence yields a higher efficiency in the three diffraction spots. This can be seen in Figs. 5(j) and 5(k), where in the inversion approach, 21% of the intensity of the first zone plate order goes to each of the three spots, whereas it is 29% in each spot for the pattern shift approach. We measured an efficiency of ~6% in the order $m = 1$, which is split according to the splitting ratios as described above.

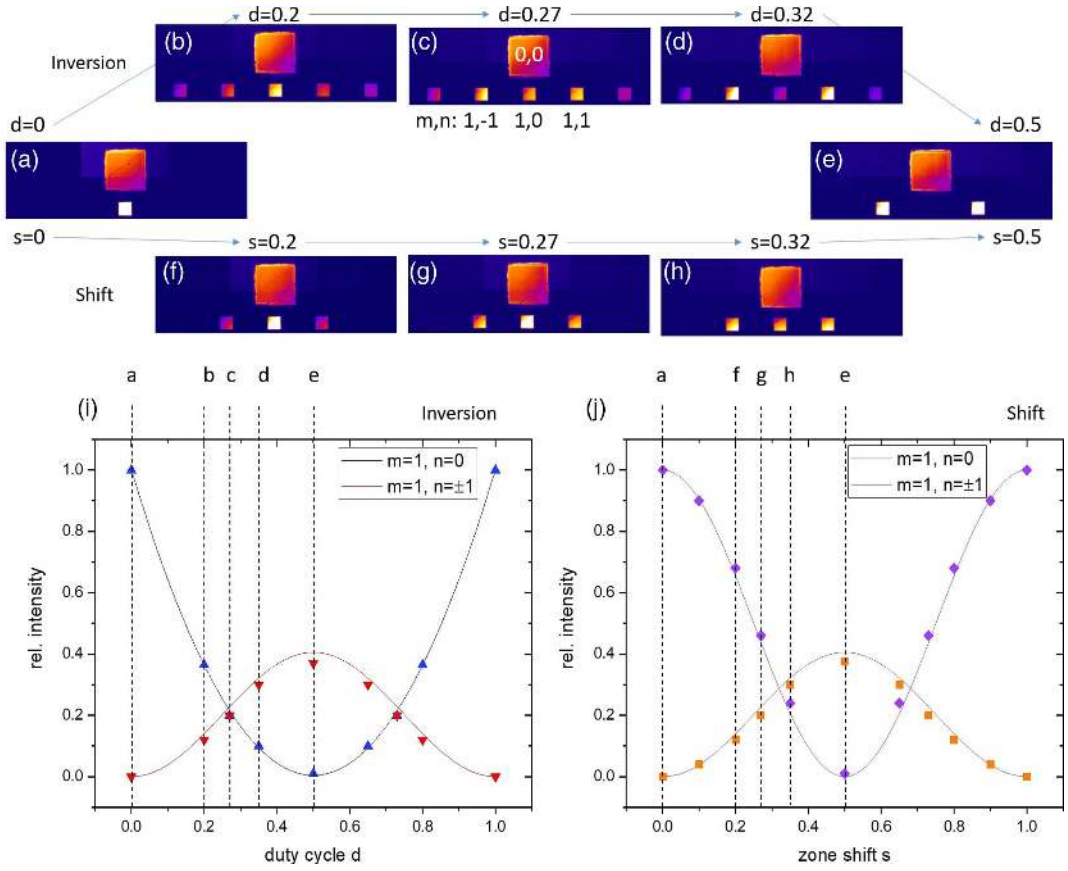

Fig. 5. Relative intensity profiles generated by the different multifocus zone plates for (a) $d = 0$, (b) $d = 0.2$, (c) $d = 0.27$, (d) $d = 0.32$, and (e) $d = 0.5$ using the pattern inversion approach, and (f) $s = 0.2$, (g) $s = 0.27$, and (h) $s = 0.32$ using pattern shift approach. The relative intensities for (j) the inversion design and (k) the shifted design obtained from the measurements (symbols) compared to the calculations (solid lines). The vertical axes were normalized to an intensity of 1 for $m = 1$, $n = 0$, and $d = s = 0$. Dashed lines mark the corresponding positions of the multifocus zone plates of (a)–(h). Note that higher orders are effectively suppressed in the pattern shift design making it better suited for a three-spot application. Please note that the intensity gradient within the illuminated squares is due to an inhomogeneity of the incoming beam caused by an alignment issue and is not a property of the optics.

4. CONCLUSIONS AND OUTLOOK

In this work, we demonstrated the properties of beam-splitting focusing optics and discussed their possible applications in XFEL experiments. Such optics are a combination of an off-axis zone plate and a phase grating that are superimposed by design. This beam-splitting grating allows us to split the beam in multiple parts, where the individual intensities of chosen diffraction orders can be controlled by choosing a different duty cycle or shift of the grating. Since the off-axis zone plate has zones that diffract perpendicular to the beam-splitting direction, it acts as a focusing device, producing in particular spatially separated zeroth and first orders. In that way, focusing to different spots without the need for an order-sorting aperture or beam stop becomes possible.

By combining both optical elements in one composite optics, the absorption losses are strongly reduced, alignment is much easier, and the grating can be designed as a perfect phase grating by inverting the written structure of the zone plate or by shifting the zones in a periodic pattern. Implementing an additional phase grating simply by design into another diffractive optical element yields huge advantages in control of beam intensities, as the phase-shifting properties do not depend on mechanical properties like etching depth, material constants, or the photon energy. In the future, such optics can be widely used for different applications at XFELs, synchrotrons, and lab sources. The benefit for XFEL science has already been proven in two user experiments. In an experiment at the DiProI beamline at FERMI, the two-spot scheme using a superimposed grating of duty cycle of $d = 0.5$ or shift of $s = 0.5$ was used in a time-streaking experiment with two incident energies [34]. The same approach enabled the first user experiment at the SCS beamline at the European XFEL. Splitting the beam in two spots, one copy for probing and one as reference, allows, in a more general picture, the normalization of spectroscopic data to account for intensity fluctuations that are inherent to free-electron lasers, in particular those that work with self-amplified spontaneous emission. In both user experiments the Si structures resisted the intensity of the XFELs without any observable damage. Adjustment of the duty cycle of the overlaying grating to $d = 0.27$ or $s = 0.32$ splits the beam in three focused parts of the same intensity. This scheme is useful to obtain quantitative absorption data. Experiments that profit in particular from this scheme are ultrafast pump-probe experiments, where one beam copy probes the pumped material, another copies the unpumped material, while the third copy acts as a reference beam.

In summary, this scheme strongly improves spectroscopy at XFELs and has a unique potential for future applications in steady-state as well as ultrafast experiments at XFELs, synchrotrons, and lab sources such as high-harmonic-generation sources.

Funding. Horizon 2020 Framework Programme (654360, 701647).

Acknowledgment. We thank A. Bergamaschi and S. Chiriotti for their assistance with the operation of the MOENCH detector. This work received funding from the EU-H2020 Research and Innovation Programme under the Marie Skłodowska-Curie grant agreement No. 701647 and No. 654360 NFFA-Europe. Part of this work was performed at the Surfaces Interfaces: Microscopy (SIM) beamline at the Swiss Light Source (SLS), Paul Scherrer Institute (PSI), Villigen, Switzerland. We gratefully acknowledge the support of the team at the DiProI beamline around Flavio Capotondi, and Emmanuelle Jal for their support in testing of our new optical element in a beamtime (proposal No. 20184077). We thank the team of the Spectroscopy and Coherent Scattering beamline led by Andreas Scherz at the European XFEL for their support and especially our local contact Loïc Le Guyader for the coordination. We further acknowledge all members of the open community proposals No. 2170 on "Efficient x-ray absorption spectroscopy at FELs: from non-perturbing fluences to non-linear effects" led by Martin Beye and No. 2161 on "On femtosecond time-resolved soft x-ray absorption spectroscopy of magnetically ordered transition metals and oxides" led by Andrea Eschenlohr for discussions on the requirements for our optics and for using them during scientific studies.

Disclosures. The authors declare no conflicts of interest.

See Supplement 1 for supporting content.

REFERENCES

1. P. Emma, R. Akre, J. Arthur, R. Bionta, C. Bostedt, J. Bozek, A. Brachmann, P. Bucksbaum, R. Coffee, F.-J. Decker, Y. Ding, D. Dowell, S. Edstrom, A. Fisher, J. Frisch, S. Gilevich, J. Hastings, G. Hays, Ph. Hering, Z. Huang, R. Iverson, H. Loos, M. Messerschmidt, A. Miahnahri, S. Moeller, H.-D. Nuhn, G. Pile, D. Ratner, J. Rzepiela, D. Schultz, T. Smith, P. Stefan, H. Tompkins, J. Turner, J. Welch, W. White, J. Wu, G. Yocky, and J. Galayda, "First lasing and operation of an angstrom-wavelength free-electron laser," Nat. Photonics **4**, 641–647 (2010).
2. G. Geloni, E. Saldin, L. Samoylova, E. Schneidmiller, H. Sinn, Th. Tschentscher, and M. Yurkov, "Coherence properties of the European XFEL," New J. Phys. **12**, 035021 (2010).
3. E. Allaria, R. Appio, L. Badano, W. A. Barletta, S. Bassanese, S. G. Biedron, A. Borga, E. Busetto, D. Castronovo, P. Cinquegrana, S. Cleva, D. Cocco, M. Cornacchia, P. Craievich, I. Cudin, G. D'Auria, M. Dal Forno, M. B. Danailov, R. De Monte, G. De Ninno, P. Delgiusto, A. Demidovich, S. Di Mitri, B. Diviacco, A. Fabris, R. Fabris, W. Fawley, M. Ferianis, E. Ferrari, S. Ferry, L. Froehlich, P. Furlan, G. Gaio, F. Gelmetti, L. Giannessi, M. Giannini, R. Gobessi, R. Ivanov, E. Karantzoulis, M. Lonza, A. Lutman, B. Mahieu, M. Milloch, S. V. Milton, M. Musardo, I. Nikolov, S. Noe, F. Parmigiani, G. Penco, M. Petronio, L. Pivetta, M. Predonzani, F. Rossi, L. Rumiz, A. Salom, C. Scafuri, C. Serpico, P. Sigalotti, S. Spampinati, C. Spezzani, M. Svandrlik, C. Svetina, S. Tazzari, M. Trovo, R. Umer, A. Vascotto, M. Veronese, R. Visintini, M. Zaccaria, D. Zangrando, and M. Zangrando, "Highly coherent and stable pulses from the FERMI seeded free-electron laser in the extreme ultraviolet," Nat. Photonics **6**, 699–704 (2012).
4. S. Schorb, D. Rupp, M. L. Swiggers, R. N. Coffee, M. Messerschmidt, G. Williams, J. D. Bozek, S.-I. Wada, O. Kornilov, T. Möller, and C. Bostedt, "Size-dependent ultrafast ionization dynamics of nanoscale samples in intense femtosecond x-ray free-electron-laser pulses," Phys. Rev. Lett. **108**, 233401 (2012).
5. S. Mukamel, D. Abramavicius, L. Yang, W. Zhuang, I. V. Schweigert, and D. V. Voronine, "Coherent multidimensional optical probes for electron correlations and exciton dynamics: from NMR to x-rays," Acc. Chem. Res. **42**, 553–562 (2009).
6. J. D. Biggs, Y. Zhang, D. Healion, and S. Mukamel, "Watching energy transfer in metalloporphyrin heterodimers using stimulated x-ray Raman spectroscopy," Proc. Natl. Acad. Sci. USA **110**, 15597–15601 (2013).
7. K. E. Dorfman, Y. Zhang, and S. Mukamel, "Coherent control of long-range photoinduced electron transfer by stimulated x-ray Raman processes," Proc. Natl. Acad. Sci. USA **113**, 10001–10006 (2016).
8. M. Buzzi, M. Makita, L. Howald, A. Kleibert, B. Vodungbo, P. Maldonado, J. Raabe, N. Jaouen, H. Redlin, K. Tiedtke, P. M. Oppeneer, C. David, F. Nolting, and J. Lüning, "Single-shot monitoring of ultrafast processes via x-ray streaking at a free electron laser," Sci. Rep. **7**, 7253 (2017).
9. D. P. Bernstein, Y. Acremann, A. Scherz, M. Burkhardt, J. Stöhr, M. Beye, W. F. Schlotter, T. Beeck, F. Sorgenfrei, A. Pietzsch, W. Wurth, and A. Föhlisch, "Near edge x-ray absorption fine structure spectroscopy with x-ray free-electron lasers," Appl. Phys. Lett. **95**, 134102 (2009).
10. R. Neutze and K. Moffat, "Time-resolved structural studies at synchrotrons and x-ray free electron lasers: opportunities and challenges," Curr. Opin. Struc. Biol. **22**, 651–659 (2012).
11. D. Zhua, M. Cammaratab, J. M. Feldkamp, D. M. Fritz, J. B. Hastings, S. Leec, H. T. Lemke, A. Robert, J. L. Turner, and Y. Fenga, "A single-shot transmissive spectrometer for hard x-ray free electron lasers," Appl. Phys. Lett. **101**, 034103 (2012).
12. T. Kroll, J. Kern, M. Kubin, D. Ratner, S. Gul, F. D. Fuller, H. Löchel, J. Krzywinski, A. Lutman, Y. Ding, G. L. Dakovski, S. Moeller, J. J. Turner, R. Alonso-Mori, D. L. Nordlund, J. Rehanek, C. Weniger, A. Firsov, M. Brzhezinskaya, R. Chatterjee, B. Lassalle-Kaiser, R. G. Sierra, H. Laksmono, E. Hill, A. Borovik, A. Erko, A. Föhlisch, R. Mitzner, V. K. Yachandra, J. Yano, P. Wernet, and U. Bergmann, "X-ray absorption spectroscopy using a self-seeded soft x-ray free-electron laser," Opt. Express **24**, 22469–22480 (2016).
13. T. Katayama, Y. Inubushi, Y. Obara, T. Sato, T. Togashi, K. Tono, T. Hatsui, T. Kameshima, A. Bhattacharya, Y. Ogi, N. Kurahashi, K. Misawa, T. Suzuki, and M. Yabashi, "Femtosecond x-ray absorption spectroscopy with hard x-ray free electron laser," Appl. Phys. Lett. **103**, 131105 (2013).
14. G. Brenner, S. Dziarzhytski, P. S. Miedema, B. Rösner, C. David, and M. Beye, "Normalized single-shot x-ray absorption spectroscopy at a free-electron laser," Opt. Lett. **44**, 2157–2160 (2019).
15. C. Chang, P. Naulleau, E. Anderson, K. Rosfjord, and D. Attwood, "Diffractive optical elements based on Fourier optical techniques: a new class of optics for extreme ultraviolet and soft x-ray wavelengths," Appl. Opt. **41**, 7384–7389 (2002).
16. U. Vogt, M. Lindblom, P. A. C. Jansson, T. T. Tuohimaa, A. Holmberg, H. M. Hertz, M. Wieland, and T. Wilhein, "Towards soft x-ray phase-sensitive imaging with diffractive optical elements," in *IPAP Conference Series* (2006), Vol. **7**, pp. 91–93.
17. C. Chang, A. Sakdinawat, P. Fischer, E. Anderson, and D. Attwood, "Single-element objective lens for soft x-ray differential interference contrast microscopy," Opt. Lett. **31**, 1564–1566 (2006).
18. M. Lindblom, T. Tuohimaa, A. Holmberg, T. Wilhein, H. M. Hertz, and U. Vogt, "High-resolution differential interference contrast x-ray zone plates: design and fabrication," Spectrochim. Acta B **62**, 539–543 (2007).
19. H. W. Schnopper, L. P. Van Speybroeck, J. P. Delvaille, A. Epstein, E. Källne, R. Z. Bachrach, J. Dijkstra, and L. Lantward, "Diffraction grating transmission efficiencies for XUV and soft x rays," Appl. Opt. **16**, 1088–1091 (1977).
20. J. Kirz, "Phase zone plates for x rays and the extreme UV," J. Opt. Soc. Am. **64**, 301–309 (1974).
21. M. Henzler and W. Göppel, *Oberflächenphysik des Festkörpers* (B. G. Teubner, 1994).
22. C. David, S. Gorelick, S. Rutishauser, J. Krzywinski, J. Vila-Comamala, V. A. Guzenko, O. Bunk, E. Färm, M. Ritala, M. Cammarata, D. M. Fritz, R. Barrett, L. Samoylova, J. Grünert, and H. Sinn, "Nanofocusing of hard x-ray free electron laser pulses using diamond based Fresnel zone plates," Sci. Rep. **1**, 57 (2011).
23. P. R. Ribič, B. Rösner, D. Gauthier, E. Allaria, F. Döring, L. Foglia, L. Giannessi, N. Mahne, M. Manfredda, C. Masciovecchio, R. Mincigrucci, N. Mirian, E. Principi, E. Roussel, A. Simoncig, S. Spampinati, C. David, and G. De Ninno, "Extreme-ultraviolet vortices from a free-electron laser," Phys. Rev. X **7**, 031036 (2017).

24. J. Vila-Comamala, K. Jefimovs, J. Raabe, B. Kaulich, and C. David, "Silicon Fresnel zone plates for high heat load x-ray microscopy," Microelectron. Eng. **85**, 1241–1244 (2008).
25. F. Marschall, Z. Yin, J. Rehanek, M. Beye, F. Döring, K. Kubiček, D. Raiser, S. Thekku Veedu, J. Buck, A. Rothkirch, B. Rösner, V. A. Guzenko, J. Viefhaus, C. David, and S. Techert, "Transmission zone plates as analyzers for efficient parallel 2D RIXS-mapping," Sci. Rep. **7**, 8849 (2017).
26. F. Döring, F. Marschall, Z. Yin, B. Rösner, M. Beye, P. Miedema, K. Kubicek, L. Glaser, D. Raiser, J. Soltau, V. A. Guzenko, J. Viefhaus, J. Buck, M. Risch, S. Techert, and C. David, "1D-full field microscopy of elastic and inelastic scattering with transmission off-axis Fresnel zone plates," Microsc. Microanal. **24**, 182–183 (2018).
27. F. Döring, M. Risch, B. Rösner, M. Beye, P. Busse, K. Kubiček, L. Glaser, P. S. Miedema, J. Soltau, D. Raiser, V. A. Guzenko, L. Szabadics, L. Kochanneck, M. Baumung, J. Buck, C. Jooss, S. Techert, and C. David, "A zone-plate-based two-color spectrometer for indirect x-ray absorption spectroscopy," J. Synchrotron Radiat. **26**, 1266–1271 (2019).
28. B. Rösner, F. Döring, P. R. Ribič, D. Gauthier, E. Principi, C. Masciovecchio, M. Zangrando, J. Vila-Comamala, G. De Ninno, and C. David, "High resolution beam profiling of x-ray free electron laser radiation by polymer imprint development," Opt. Express **25**, 30686–30695 (2017).
29. C. David, B. Rösner, F. Döring, V. Guzenko, F. Koch, M. Lebugle, F. Marschall, G. Seniutinas, J. Raabe, B. Watts, D. Grolimund, Z. Yin, M. Beye, S. Techert, J. Viefhaus, G. Falkenberg, and C. Schroer, "Diffractive x-ray optics for synchrotrons and free-electron lasers," Microsc. Microanal. **24**, 264–267 (2018).
30. E. Jal, M. Makita, B. Rösner, C. David, F. Nolting, J. Raabe, T. Savchenko, A. Kleibert, F. Capotondi, E. Pedersoli, L. Raimondi, M. Manfredda, I. Nikolov, X. Liu, A. el dine Merhe, N. Jaouen, J. Gorchon, G. Malinowski, M. Hehn, B. Vodungbo, and J. Lüning, "Single-shot time-resolved magnetic x-ray absorption at a free-electron laser," Phys. Rev. B **99**, 144305 (2019).
31. U. Flechsig, F. Nolting, A. Fraile Rodríguez, J. Krempaský, C. Quitmann, T. Schmidt, S. Spielmann, and D. Zimoch, "Performance measurements at the SLS SIM beamline," AIP Conf. Proc **1234**, 319–322 (2010).
32. G. Olivieri, A. Goel, A. Kleibert, and M. A. Brown, "Effect of x-ray spot size on liquid jet photoelectron spectroscopy," J. Synchrotron Radiat. **22**, 1528–1530 (2015).
33. A. Bergamaschi, M. Andrä, R. Barten, C. Borca, M. Brückner, S. Chiriotti, R. Dinapoli, E. Fröjdh, D. Greiffenberg, T. Huthwelker, A. Kleibert, M. Langer, M. Lebugle, C. Lopez-Cuenca, D. Mezza, A. Mozzanica, J. Raabe, S. Redford, C. Ruder, V. Scagnoli, B. Schmitt, X. Shi, U. Staub, D. Thattil, G. Tinti, C. F. Vaz, S. Vetter, J. Vila-Comamala, and J. Zhang, "The MÖNCH detector for soft x-ray, high-resolution, and energy resolved applications," Synchrotron Radiat. News **31**(6), 11–15 (2018).
34. B. Rösner, B. Vodungbo, V. Chardonnet, F. Döring, V. A. Guzenko, M. Hennes, A. Kleibert, M. Lebugle, J. Lüning, N. Mahne, A. Merhe, D. Naumenko, I. P. Nikolov, I. Lopez-Quintas, E. Pedersoli, P. R. Ribič, T. Savchenko, B. Watts, M. Zangrando, F. Capotondi, C. David, and E. Jal, "Simultaneous two-color snapshot view on ultrafast charge and spin dynamics in a Fe–Cu–Ni tri-layer," arXiv:2005.10611 (2020).